J Mater Sci (2007) 42:9200–9204
DOI 10.1007/s10853-007-1913-2

Synthesis of $(Y, Gd)_3Al_5O_{12}$:Ce nanophosphor by co-precipitation method and its luminescence behavior

Kai Zhang · Hezhou Liu · Yating Wu · Wenbin Hu

Received: 28 June 2006 / Accepted: 4 June 2007 / Published online: 27 July 2007

Abstract $(Y, Gd)_3Al_5O_{12}$:Ce nanophosphor was synthesized by co-precipitation method using the mixture solution of ammonium liquor and ammonium hydrogen carbonate as precipitant. The effect of Ce and Gd concentration on the crystallization and luminescence behavior of the phosphor was studied. The results indicate $(Y, Gd)_3Al_5O_{12}$:Ce nanophosphor is obtained after the precipitates are sintered at 1,000 °C for 2 h. Following the increase of Ce and Gd concentration, the emission shows red shift.

Introduction

Trivalent cerium activated yttrium aluminum garnet (YAG:Ce) has been found to be suitable for converting the blue light emitting diodes (LEDs) radiation into a very broad band yellow emission [1], which provides a basis to use YAG:Ce phosphors along with GaN LEDs to produce white light emitting diodes (WLEDs). Compared with traditional lighting, WLEDs have more advantages of high energy-efficiency, high reliability, long life, fast response, and non-polluting. It is suggested that there would be a prosperous future in lamp market. Because of different manufacturing technologies, the emission peak of GaN LEDs varies from 450 to 480 nm. Consequently, it is necessary to adjust YAG:Ce emission to match GaN LEDs. Rare earths doping is an effective way to improve YAG:Ce emission [2].

The YAG-based materials are normally synthesized at a relatively high temperature by a solid-state reaction between Al_2O_3 and Y_2O_3 to reduce intermediate phases, such as YAM ($Y_4Al_2O_9$) and YAP ($YAlO_3$) [3]. However, it leads to large, wide-varying particle sizes and needs ball-milling, which deteriorates the luminescence properties. The co-precipitation method, because of its apparent advantages of homogeneity, high reactivity of starting materials and lower sintering temperature, is a novel process to synthesize ultrafine powders [4].

In this study, ammonium hydrogen carbonate and ammonia liquor were used to synthesize $(Y, Gd)_3Al_5O_{12}$ powders via co-precipitation. The crystalline-phase compositions, thermal decomposition, particle sizes, morphologies, and luminescence properties of the synthesized powders were evaluated.

Experimental

Materials

The initial materials for $(Y, Gd)_3Al_5O_{12}$ phosphors included rare earth oxides Y_2O_3 (99.999%), Gd_2O_3 (99.999%), $Ce(NO_3)_3 \cdot 6H_2O$ (A.R.) and $Al(NO_3)_3 \cdot 9H_2O$ (A.R.).

Y_2O_3 and Gd_2O_3 were dissolved in dilute HNO_3 and the solution was evaporated to remove the surplus HNO_3. $Ce(NO_3)_3 \cdot 6H_2O$ and $Al(NO_3)_3 \cdot 9H_2O$ was dissolved in deionized water. The mother salt solution was prepared according to stoichiometric proportion of $(Y_{1-x}Gd_x)_{3-y}Al_5O_{12}$:$y$Ce ($x$ = 0–1, y = 0.03–0.3). The precipitant solution was composed of ammonium hydrogen carbonate and ammonia liquor at the mole ratio about 1:3.

K. Zhang · H. Liu · Y. Wu · W. Hu (✉)
State Key Laboratory of Metal Matrix Composites,
Shanghai Jiaotong University, Shanghai 200030, China
e-mail: material_hu@163.com

Powder synthesis

For multi-cation materials, the reverse-strike technique (adding mother salt solution to the precipitant solution) has the advantage of higher cation homogeneity in the precursors [5] and was used in this study. Precursors were produced by dropping the mother salt solution at a speed of 3 mL/min into the precipitant solution under a magnetic stirring at room temperature. It was stirred another 30 min after dropping. The resultant suspension, after aging for 8 h, was filtered, washed four times with deionized water, rinsed with ethyl alcohol, and dried at 120 °C over 10 h. After finely milled in an agate mortar, the precursors were preheated at 500 °C for 2 h in air and then additionally sintered at 1,000 °C for 2 h in a weakly reducing atmosphere consisting of nitrogen–hydrogen mixture containing 8% volume of hydrogen.

Powder characterization

Differential scanning calorimetry (DSC) of the original precursors were conducted on a DSC analyzer (Model C404/6/7, NETZSCH-Gerätebau, Selb, Germany) in flowing nitrogen atmosphere with a heating rate of 10 °C/min. Thermal gravimetric analysis (TG) of the original precursors were carried out by a TG analyzer (Mode TGA 1000, USA) in flowing nitrogen with a heating rate of 10 °C/min.

Powder morphologies were observed by field emission scanning electron microscopy (FESEM, Model FEI—Sirion 200, Philips, Netherlands). For powders, sample was ultrasonically dispersed into acetone, and the suspension was spread on the surface of copper plate. All samples were coated with a thin layer of aurum for good conductivity before observation.

Phase identification was performed on a Rigaku D/Max X-ray diffractometer (XRD) using nickel filtered CuK_{α} radiation in the range of $2\theta = 10$–70° with a scanning speed of 6°2θ per min.

The excitation and emission spectra were analyzed on a LS 50B luminescence spectrometer at room temperature.

Results and discussion

Phase transition during sintering

X-ray diffractometer spectra of precursors composition of $Y_{2.95}Al_5O_{12}$:0.05Ce sintered at 500 and 1,000 °C are shown in Fig. 1a. The precursors crystallized as pure YAG at 1,000 °C, that is, about 600 °C lower than required for the constituent oxide mixtures [6]. Thus, the homogeneous mixing of the precursor powders in the sample significantly enhanced the garnet phase formation. Furthermore, because of the similar radii of Y^{3+} and Ce^{3+}, small quantity substitution of Ce^{3+} for Y^{3+} did not affect the cubic structure of YAG.

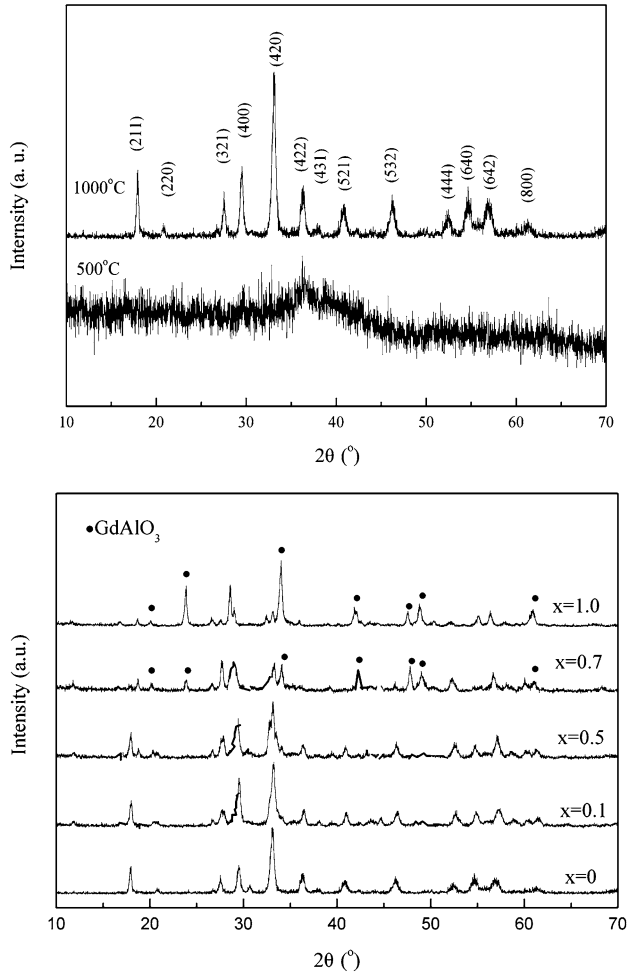

Fig. 1 XRD spectra of $Y_{2.95}Al_5O_{12}$:0.05Ce sintered at 500 and 1,000 °C (**a**), $(Y_{1-x}Gd_x)_{2.85}Al_5O_{12}$:0.15Ce sintered at 1,000 °C (**b**)

X-ray diffractometer spectra of a series of Gd doped YAG:Ce sintered at 1,000 °C are shown in Fig. 1b.Up to 50 mol% Gd^{3+} additions, the sintered powders remain YAG structure. As more Y^{3+} was replaced, other phases appeared. The main new phase was $GdAlO_3$. In the case of conventional solid-state synthesis, the YAG phase generation proceeds by a series of reactions as follows:

$$2Y_2O_3 + Al_2O_3 \rightarrow Y_4Al_2O_9 \quad (1)$$

$$Y_4Al_2O_9 + Al_2O_3 \rightarrow 4YAlO_3 \quad (2)$$

$$3YAlO_3 + Al_2O_3 \rightarrow Y_3Al_5O_{12}. \quad (3)$$

The reaction proceeds by the diffusion of Al into Y_2O_3 grains [7]. Compared with Y_2O_3 grains, electron density

distribution and crystal structure of Gd_2O_3 grains made it more difficult diffusion of Al in Gd_2O_3 grains. When the Gd doping content increase, the series of reactions stayed in the second step, thus $GdAlO_3$ was formed.

Thermal analysis

DSC/TG traces of the precursors, which had a composition of $Y_{2.95}Al_5O_{12}$:0.05Ce are given in Fig. 2. The endothermic peak at about 100 °C was due to the evaporation of alcohol and desorption of the absorbed water. The endothermic peak at about 180 °C resulted from removal of crystal water. The exothermic peak at 330 °C was assigned to pyrolysis of ammonia. The sharp exothermic peak at 920 °C was caused by crystallization of YAG, which is evidenced by the XRD results in Fig. 1a. The major mass loss of the precursor occurred below 500 °C.

Powder morphologies

Figure 3 shows FESEM morphologies of (Y, Gd)$_3$Al$_5$O$_{12}$ powders. The precursors were composed of extremely fine particles. The particles were basically spherical in shape. The precursors showed mild agglomeration. The size of particle was about 20 nm. After sintered at 1,000 °C, particles merged. Shape of particles became irregular and particle sizes distribution slight widened. The mean size of phosphor powders was about 40 nm.

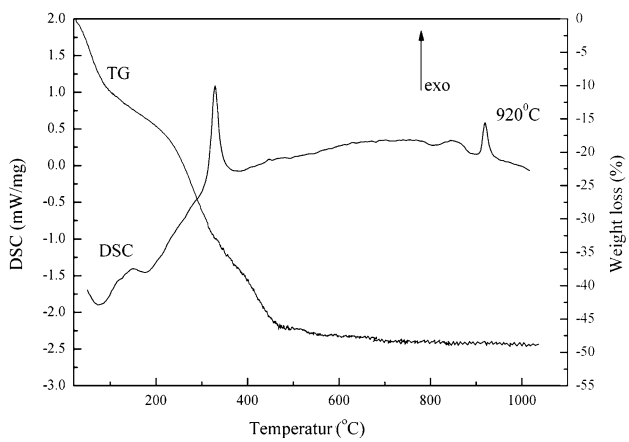

Fig. 2 DSC/TG traces of $Y_{2.95}Al_5O_{12}$:0.05Ce precursors

Luminescence properties of (Y, Gd)$_3$Al$_5$O$_{12}$:Ce

The emission of Ce^{3+} occurs from the lowest crystal field component of $5d^1$ configuration to the two levels of the ground state $^2F_{5/2}$ and $^2F_{7/2}$, which is separated by 2,200 cm^{-1} due to spin-orbit coupling [8]. Unlike the 4f electron with the shielding effect of outer shell 6s and 5p electrons, the 5d state is split by crystal field and hence the d–f emission band of Ce^{3+} is heavily dependent on the local crystal field surrounding the Ce^{3+}. Thus, the emission is very sensitive to crystallographic environment, which results in red or blue shift of Ce^{3+} emission.

Figure 4 shows excitation spectra of different concentration Ce^{3+} doped YAG. The maximum of excitation band was around 460 nm.

Figure 5 shows the emission intensity and maximum of emission band vary with different Ce^{3+} concentration. The maximum intensity was achieved for about 4.8 mol% Ce^{3+} additions. Concentration quenching effect was observed when Ce^{3+} amount was increased beyond this limit due to the increase of intra ionic non-radiative relaxation between adjacent Ce^{3+} ions. When the concentration of Ce^{3+} increased from 3.33 to 8.00 mol%, the maximum of Ce^{3+} emission band shifted from 513 to 535 nm. Red shift of emission occurred. The red shift of emission can be explained by magnetic interactions between neighboring Ce^{3+} ions [9].

Figure 6 shows excitation spectra of different concentration Gd^{3+} doped YAG:Ce. When the concentration of Gd^{3+} increased, the maximum of excitation band showed slight red shift.

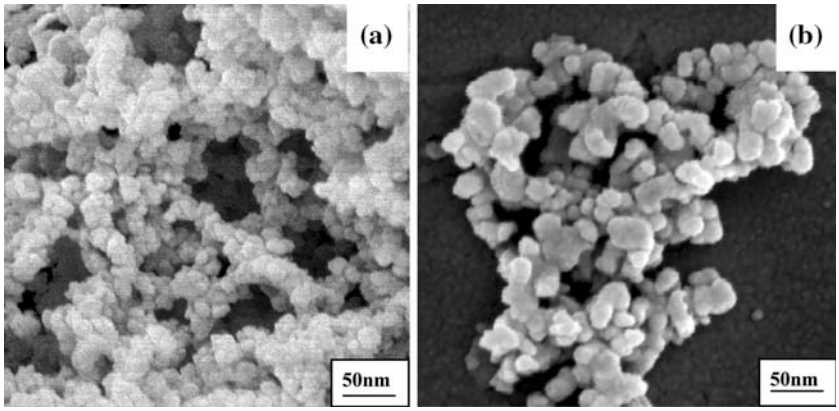

Fig. 3 FESEM morphologies of the powders: the precursors (**a**), sintered at 1,000 °C (**b**)

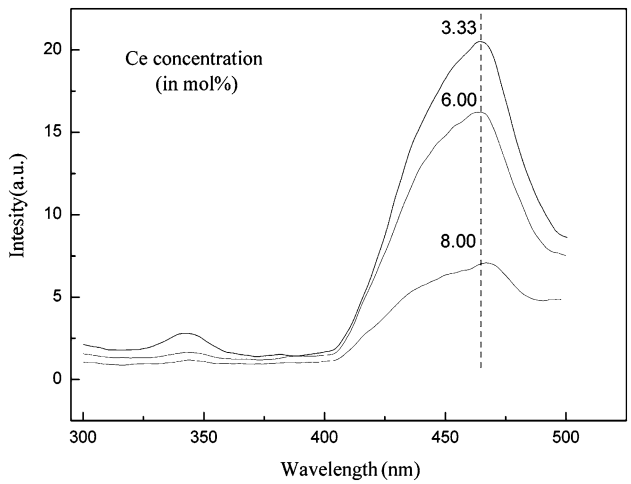

Fig. 4 Excitation spectra with different Ce^{3+} concentration (λ_{em} = 560 nm)

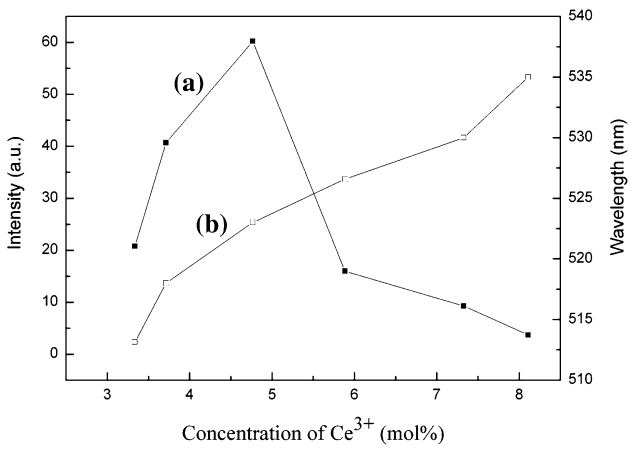

Fig. 5 The emission intensity (**a**) and maximum of emission band (**b**) vary with different Ce^{3+} concentration (λ_{ex} = 460 nm)

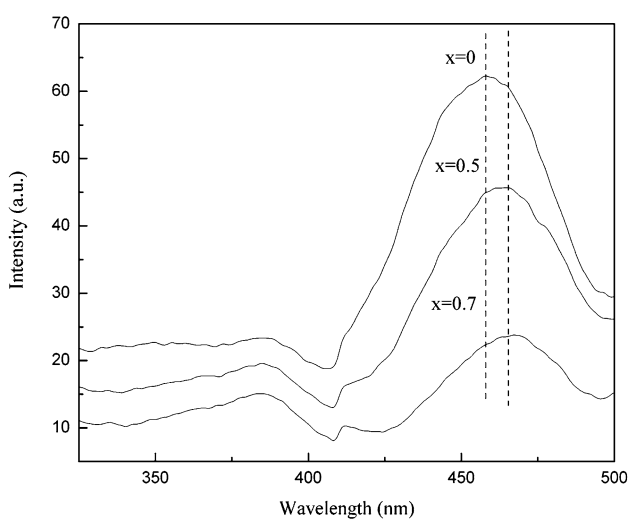

Fig. 6 Excitation spectra of $(Y_{1-x}Gd_x)_{2.85}Al_5O_{12}$:0.15Ce ($\lambda_{em}$ = 560 nm)

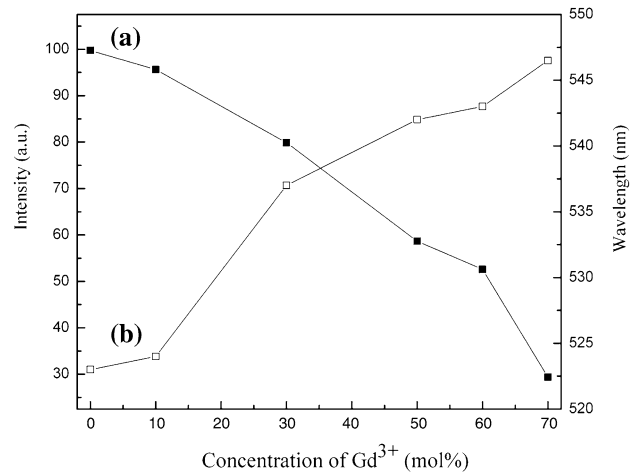

Fig. 7 The emission intensity (**a**) and maximum of emission band (**b**) vary with different Gd^{3+} concentration (λ_{ex} = 460 nm)

Figure 7 shows the emission intensity and maximum of emission band varying with the Gd^{3+} concentration. As the concentration of Gd^{3+} increased, the maximum emission band shifted from 523 to 546 nm, while the emission intensity decreased. The red shift implied that the lowest 5d component for Ce^{3+} became lower as the concentration of Gd^{3+} increased [10], i.e., the split width of the Ce^{3+} 5d level was larger, indicating that the crystal field became stronger following the doing concentration of Gd^{3+} increased. Until 50 mol% Gd^{3+} additions, the emission intensity nearly linearly decreased. When 70 mol% Gd^{3+} doing, the emission intensity sharply decreased because of other phases emerging.

Conclusions

A series of $(Y_{1-x}Gd_x)_{3-y}Al_5O_{12}$:$y$Ce ($x$ = 0–1, y = 0.03–0.3) phosphor was prepared by co-precipitation processing using the mixture of ammonium hydrogen carbonate and ammonia liquor as precipitant. The precursors were basically spherical in shape and the size of precursors was about 20 nm. After sintered at 1,000 °C, the precursors crystallized as pure YAG. Shape of sintered powders became irregular and particle sizes slight widened. Small quantity substitution of Ce^{3+} for Y^{3+} did not affect YAG structure of the phosphor powders. When Y^{3+} was replaced by Gd^{3+} beyond 50 mol%, other phases appeared. The main new phase was $GdAlO_3$.

As the concentration of Ce increases, emission showed red shift. The maximum emission intensity was obtained for 4.8 mol% Ce^{3+} additions. Concentration quenching effect was observed when Ce amount was increased beyond this limit. With increment of Gd doing concentration, emission showed red shift, while the emission intensity decreased.

Acknowledgements This work was financially supported by the "Shanghai Science and Technology Development Fund (No. 0452nm046)". The authors would like to thank Instrumental Analysis Center of SJTU for sample characterization.

References

1. Lee S, Seo SY (2002) J Electrochem Soc 149:85
2. Pan YX, Wu MM, Su Q (2004) J Phys Chem Solids 65:845
3. Cockayne B, Lent B (1979) J Cryst Growth 46:371
4. Li JL, Takayasu I, Lee JH, Toshiyuki M, Yoshiyuki Y (2000) J Eur Ceram Soc 20:2395
5. Apte P, Burke H, Pickup H (1992) J Mater Res 7(3):706
6. Karin MK, Esther S, Kenneth H (1994) J Am Ceram Soc 77(11):2866
7. Matsubara I, Paranthaman M, Allison SW, Cates MR, Beshears DL, Holcomb DE (2000) Mater Res Bull 35:217
8. Blasse G, Grabmaier BC (1994) Luminescent materials. Springer, Berlin
9. Ageeth AB, Andries M (2001) J Phys Chem B 105:10197
10. Zhou YH, Lin J, Yu M, Wang SB, Zhang HG (2002) Mater Lett 56:628